

# How clustering dark energy affects matter perturbations

A. Mehrabi<sup>1\*</sup>, S. Basilakos<sup>2†</sup> and F. Pace<sup>3</sup>

<sup>1</sup> Department of Physics, Bu-Ali Sina University, Hamedan 65178, Iran

<sup>2</sup> Academy of Athens, Research Center for Astronomy & Applied Mathematics, Soranou Efessiou 4, 11-527, Athens, Greece

<sup>3</sup> Jodrell Bank Centre for Astrophysics, School of Physics and Astronomy, The University of Manchester, Manchester, M13 9PL, UK

Accepted ?, Received ?; in original form August 4, 2015

## ABSTRACT

The rate of structure formation in the Universe is different in homogeneous and clustered dark energy models. The degree of dark energy clustering depends on the magnitude of its effective sound speed  $c_{\text{eff}}^2$  and for  $c_{\text{eff}} = 0$  dark energy clusters in a similar fashion to dark matter while for  $c_{\text{eff}} = 1$  it stays (approximately) homogeneous. In this paper we consider two distinct equations of state for the dark energy component,  $w_d = \text{const}$  and  $w_d = w_0 + w_1 \left( \frac{z}{1+z} \right)$  with  $c_{\text{eff}}$  as a free parameter and we try to constrain the dark energy effective sound speed using current available data including SnIa, Baryon Acoustic Oscillation, CMB shift parameter (*Planck* and *WMAP*), Hubble parameter, Big Bang Nucleosynthesis and the growth rate of structures  $f\sigma_8(z)$ . At first we derive the most general form of the equations governing dark matter and dark energy clustering under the assumption that  $c_{\text{eff}} = \text{const}$ . Finally, performing an overall likelihood analysis we find that the likelihood function peaks at  $c_{\text{eff}} = 0$ , however the dark energy sound speed is degenerate with respect to the cosmological parameters, namely  $\Omega_m$  and  $w_d$ .

**Key words:** Methods: analytic – cosmological parameters – cosmology: theory – dark energy

## 1 INTRODUCTION

We are living in a special epoch of the cosmic history where the expansion of the Universe is accelerated due to an unknown energy component, usually dubbed dark energy (DE). This acceleration has been discovered observationally using the luminosity distance of Type Ia supernovae (SnIa) (Perlmutter et al. 1997, 1998, 1999; Riess et al. 2004; Astier et al. 2006; Jha et al. 2007). In addition to this, other observations including the cosmic microwave background (CMB) (Bennett et al. 2003; Spergel et al. 2003, 2007; Planck Collaboration XIII 2015; Planck Collaboration XIV 2015), large scale structures (LSS) (Hawkins et al. 2003; Tegmark et al. 2004; Cole et al. 2005) and baryon acoustic oscillation (BAO) (Eisenstein et al. 2005; Seo & Eisenstein 2005; Blake et al. 2011) support an accelerated expansion. At a fundamental level there are two different approaches to describe the phenomenon of the cosmic acceleration and indeed many efforts are devoted to investigate its deep nature both observationally and theoretically. One way is to consider a fluid with a sufficiently negative pressure dubbed DE and the other is based on the modification of the laws of gravity on large scales. The first approach comes in many different scenarios. The simplest one is a very tiny cosmological constant  $\Lambda$  in Einstein field equations that has a (negative) pressure equal to its energy density and equation-of-state parameter  $w_d = \frac{p_d}{\rho_d} = -1$  (Weinberg 1989;

Sahni & Starobinsky 2000; Peebles & Ratra 2003). The overall theoretical cosmological model (cosmological constant plus cold dark matter to explain galaxy rotation curves and the potential well for structure formation) is called  $\Lambda$ CDM model. Despite being highly consistent with observational data, the  $\Lambda$ CDM model suffers of two theoretical problems, namely the fine-tuning and the cosmic coincidence problem (Weinberg 1989; Sahni & Starobinsky 2000; Peebles & Ratra 2003). Differently from the cosmological constant case with equation of state (EoS)  $w_d = -1$ , other dynamical models have been largely studied in the literature and usually categorised in two branches, quintessence models (Armendariz-Picon et al. 2000; Copeland et al. 2006) and k-essence models (Armendariz-Picon et al. 1999, 2000; Chiba et al. 2000, 2009; Amendola & Tsujikawa 2010).

The simplest way to modify gravity is to consider Einstein-Hilbert Lagrangian as a generic function of the Ricci scalar  $R$  ( $f(R)$  theories, Schmidt 1990; Magnano & Sokolowski 1994; Dobado & Maroto 1995; Capozziello et al. 2003; Carroll et al. 2004) or add extra-dimension models like in the DGP model (Dvali, Gabadadze & Porrati 2000). Understanding which class of models is the real one is one of the biggest challenges for cosmology.

In addition to the background evolution, large scale structures provide valuable information about the nature of dark energy (Tegmark et al. 2004, 2006). Primordial matter perturbations grow throughout the cosmic history and their growth rate depends on the overall energy budget and on the properties of the cosmic fluids.

\* mehrabi@basu.ac.ir

† svasil@academyofathens.gr

DE slows down the growth rate of large-scale structures. Structures grow due to gravitational instability and DE acts opposing and reducing the growth rate. The growth rate of structures can be measured from the redshift space distortion (RSD). Inward peculiar velocities of large-scale structures generate a distortion that is directly related to the matter density contrast.

Since the cosmological constant does not change in space and time, it can not cluster like dark matter (DM) and it has a negligible contribution to the energy density of the universe at high redshift. On the other hand, dynamical DE can cluster and the amount of clustering depends strongly on its effective sound speed. The effective sound speed is defined as  $c_{\text{eff}}^2 = c_e = \frac{\delta p_d}{\delta \rho_d}$  (hereafter we use  $c_e$ ) where  $\delta p_d$  and  $\delta \rho_d$  are the pressure and energy density perturbations for DE respectively and coincides with the actual sound speed in the dark energy comoving rest frame (Hu 1998). In quintessence models we have  $c_e \simeq 1$  so DE perturbations can not grow on sub-horizon scales while in k-essence models the effective sound speed can be tiny ( $c_e \ll 1$ ) (Garriga & Mukhanov 1999; Armendariz-Picon et al. 1999, 2000; Babichev et al. 2006; Akhoury et al. 2011) and DE perturbations grow similarly to dark matter (DM) perturbations. The possibility of DE clustering has been studied by many authors (Erickson et al. 2002; Bean & Doré 2004; Hu & Scranton 2004; Ballesteros & Riotto 2008; de Putter et al. 2010; Sapone & Majerotto 2012; Batista & Pace 2013; Dossett & Ishak 2013; Basse et al. 2014; Batista 2014; Pace et al. 2014; Steigerwald et al. 2014). In particular, it has been shown that the homogeneous DE scenario fails to reproduce the observed concentration parameter of the massive galaxy clusters (Basilakos et al. 2009). In this framework, de Putter et al. (2010) pointed out that CMB and LSS slightly prefer dynamical DE with  $c_e \neq 1$  and recently Mehrabi, Malekjani & Pace (2015) and Basilakos (2015) have shown that clustering DE reproduces the growth data better in the framework of the spherical collapse model. A similar conclusion was suggested also by Nesseris & Sapone (2014).

The growth rate  $f = \frac{d \ln \delta_m}{d \ln a}$  is usually approximated by  $f = \Omega_m^\gamma$  as first introduced by Peebles (1993). In this parametrization  $\gamma$  is the so called growth index and can be used to distinguish between DE and modified gravity models (Linder 2005; Huterer & Linder 2007; Basilakos & Pouri 2012; Rapetti et al. 2013). It is well known that for a  $\Lambda$ CDM model  $\gamma$  is independent of redshift and equal to 6/11. The evolution of the matter density  $\Omega_m$  depends on the evolution of the Hubble parameter  $H(a)$  and hence on the particular cosmological model adopted. In this paper we consider two distinct models, a constant  $w_d$  and a dynamical  $w_d(z)$ , and we consider  $c_{\text{eff}}$  as a free parameter. Then based on the linear regime we numerically solve the perturbed general relativity (GR) equations to evaluate the growth rate of matter in the presence of DE clustering. Using a Markov Chain Monte Carlo (MCMC) method we can constrain the cosmological parameters using SNIa, BAO, CMB shift parameter, the Hubble parameter, the Big Bang Nucleosynthesis (BBN) and growth rate data  $f\sigma_8(z)$ .

The structure of this paper is as follows. In section 2 we derive the equations governing the linear growth of matter perturbations in a general relativistic framework and show the effects of DE clustering on the growth rate of matter. In section 3 we present all the details of the observational data used in this work to constrain the cosmological parameters including the DE sound speed and their uncertainties. In section 4, we provide for the first time (to our knowledge) an approximated solution of the growth index of matter fluctuations as a function of the cosmological param-

eters, DE perturbations and  $c_e$ . Finally in section 5 we conclude and discuss our results.

## 2 EFFECT OF DARK ENERGY SOUND SPEED ON THE GROWTH RATE OF MATTER PERTURBATIONS

In this section we revise the fundamental equations necessary to our analysis. The sound horizon of DE with effective sound speed  $c_e$  in a FRW universe is given by:

$$\lambda_s(a) = \int_{a_i}^a \frac{c_e(x)}{x\mathcal{H}(x)} dx, \quad (1)$$

where  $\mathcal{H} = \frac{a'}{a}$ , the prime being the derivative with respect to conformal time ( $\eta$ ) and  $a_i$  an initial scale factor. The nominal Hubble parameter is given by  $H = \frac{\dot{a}}{a}$  and thus  $\mathcal{H} = aH$  which implies

$$\frac{\mathcal{H}'}{\mathcal{H}^2} = 1 + \frac{\dot{\mathcal{H}}}{\mathcal{H}^2}, \quad (2)$$

where an overdot refers to a derivative with respect to the cosmic time ( $t$ ). In the case of  $c_e \simeq 1$ , pressure suppresses any DE perturbation with the consequence that DE may cluster only on scales comparable to the horizon.

The opposite situation holds if  $c_e \ll 1$ . Indeed in this case DE can cluster in analogy to the DM component and perturbations will grow with time. DE clustering modifies the evolution of DM perturbation and thus it affects the rate of structure formation in the universe.

We start our derivation of the relevant equations by considering the line element of an expanding universe in the Newtonian gauge without anisotropic stress:

$$ds^2 = -(1 + 2\phi)dt^2 + a^2(t)(1 - 2\phi)d\vec{x}^2, \quad (3)$$

where  $\phi$  is the Bardeen potential. First-order Einstein equations in Fourier space are:

$$\begin{aligned} 3\mathcal{H}\phi' + (3\mathcal{H}^2 + k^2)\phi &= -\frac{3\mathcal{H}^2}{2}(\Omega_m\delta_m + \Omega_d\delta_d) \quad (4) \\ \phi'' + 3\mathcal{H}\phi' + \left(\frac{2a''}{a} - \mathcal{H}^2\right)\phi &= \frac{3\mathcal{H}^2}{2}\Omega_d\frac{\delta p_d}{\delta\rho_d}\delta_d, \quad (5) \end{aligned}$$

where  $\Omega_m = \Omega_{\text{DM}} + \Omega_b$  ( $\Omega_d = 1 - \Omega_m$ ) is the matter (dark energy) density parameter and  $\delta_m$  ( $\delta_d$ ) is the corresponding density contrast. The first-order energy-momentum conservation equations for a generic fluid with equation-of-state parameter  $w$  are (Ma & Bertschinger 1995)

$$\delta' = -(1+w)(\theta - 3\phi') - 3\frac{a'}{a}\left(\frac{\delta p}{\delta\rho} - w\right)\delta, \quad (6)$$

$$\theta' = -\frac{a'}{a}(1-3w)\theta - \frac{w'}{1+w}\theta + \frac{\delta p}{1+w}k^2\delta + k^2\phi. \quad (7)$$

These equations are correct for any fluid with  $p = w\rho$  (for dust  $w = 0$  and for dark energy  $w = w_d$ ), where  $\delta$  is the density contrast,  $\theta$  is the divergence of the fluid velocity ( $\theta = ik^i v_i$ ) and  $\frac{\delta p}{\delta\rho}$  can be written as (Bean & Doré 2004)

$$\frac{\delta p}{\delta\rho} = c_e + 3\mathcal{H}(1+w)(c_e - c_{\text{ad}}^2)\frac{\theta}{\delta k^2}, \quad (8)$$

where  $c_a^2 = c_a$  is the DE adiabatic sound speed:

$$c_a = w - \frac{w'}{3\mathcal{H}(1+w)}. \quad (9)$$

Note that the second term in the right hand side of Eq. (8) appears

because we demand pressure perturbations to be a gauge invariant quantity (Bean & Doré 2004). For a perfect fluid, perturbations in the pressure are purely determined by the adiabatic sound speed but for an imperfect fluid dissipative processes generate entropic perturbations and therefore we have a more general relation. In this case,  $c_e$  acts like a proxy for pressure perturbations and the growth of perturbation in the DE component depends on the effective sound speed and not on the adiabatic sound speed any more. In the following this statement will be confirmed by solving the perturbed equations numerically.

To study the effect of the DE sound speed on structure formation, we consider a universe with pressure-less DM and a DE component with varying equation of state that we specialise to  $w_d(z) = w_0 + w_1 \frac{z}{1+z}$ . The latter parametrization is the well known Chevallier-Polarski-Linder (CPL) parametrization (Chevallier & Polarski 2001; Linder 2003). We eliminate  $\theta$  from Eqs. (6) and (7) and find two second order differential equations for the density contrast of DM and DE. In addition using  $\frac{d}{d\eta} = a\mathcal{H}\frac{d}{da}$  and  $\frac{d^2}{d\eta^2} = a^2\mathcal{H}^2\frac{d^2}{da^2} + (a\mathcal{H}^2 + a\dot{\mathcal{H}})\frac{d}{da}$ , these equations can be written in terms of the scale factor. Finally our desired equations governing the growth of DM and DE perturbations are:

$$\frac{d^2\delta_m}{da^2} + A_m\frac{d\delta_m}{da} + B_m\delta_m = S_m, \quad (10)$$

$$\frac{d^2\delta_d}{da^2} + A_d\frac{d\delta_d}{da} + B_d\delta_d = S_d, \quad (11)$$

and the coefficients [see also Eq. (2)] are:

$$A_m = \frac{1}{a} \left( 2 + \frac{\mathcal{H}'}{\mathcal{H}^2} \right) = \frac{1}{a} \left( 3 + \frac{\dot{H}}{H^2} \right), \quad (12)$$

$$B_m = 0,$$

$$S_m = 3\frac{d^2\phi}{da^2} + \frac{3}{a} \left[ 2 + \frac{\mathcal{H}'}{\mathcal{H}^2} \right] \frac{d\phi}{da} - \frac{k^2}{a^2\mathcal{H}^2}\phi,$$

$$A_d = \frac{1}{a} \left[ 2 + \frac{\mathcal{H}'}{\mathcal{H}^2} + 3c_a - 6w_d \right],$$

$$B_d = \frac{1}{a^2} \left[ 3(c_e - w_d) \left( 1 + \frac{\mathcal{H}'}{\mathcal{H}^2} - 3w_d + 3c_a - 3c_e \right) + \frac{k^2}{\mathcal{H}^2}c_e - 3a\frac{dw_d}{da} \right],$$

$$S_d = (1 + w_d) \left[ 3\frac{d^2\phi}{da^2} + \frac{3}{a} \left( 2 + \frac{\mathcal{H}'}{\mathcal{H}^2} - 3c_a \right) \frac{d\phi}{da} - \frac{k^2}{a^2\mathcal{H}^2}\phi + \frac{3}{1 + w_d} \frac{d\phi}{da} \frac{dw_d}{da} \right],$$

where  $\frac{\mathcal{H}'}{\mathcal{H}^2}$  (or  $\frac{\dot{H}}{H^2}$ ) is a function of the scale factor and using Friedmann equations we have

$$\frac{\mathcal{H}'}{\mathcal{H}^2} = -\frac{1}{2} \frac{\Omega_m + \Omega_d(1 + 3w_d)}{\Omega_m + \Omega_d} = -\frac{1}{2}(1 + 3\Omega_d w_d), \quad (13)$$

These equations are not in agreement with Eq. (44) in Abramo et al. (2009), which were obtained in the limit of a matter dominated universe ( $\frac{\mathcal{H}'}{\mathcal{H}^2} = -\frac{1}{2}$ ) and a constant  $w_d$ . To resolve this discrepancy, see appendix (A).

We integrate Eqs. (10) and (11) numerically from  $z_i = 100$  to  $z = 0$ , in order to obtain the density contrast of DM and DE. We use the same procedure of Abramo et al. (2009) to find the initial conditions. In the matter dominated era  $\phi' \simeq 0$ , so from Eq. (4) we have:

$$\delta_{m,i} = -2\phi_i \left( 1 + \frac{k^2}{3\mathcal{H}_i^2} \right), \quad (14)$$

for the initial value of  $\delta_m$  and

$$\frac{d\delta_{m,i}}{da} = -\frac{2}{3} \frac{k^2}{\mathcal{H}_i^2} \phi_i, \quad (15)$$

for its derivative. For  $\delta_d$  the initial value is set using the adiabatic perturbations condition (Kodama & Sasaki 1984; Amendola & Tsujikawa 2010),

$$\delta_{d,i} = (1 + w_d)\delta_{m,i}, \quad (16)$$

and its derivative is set to

$$\frac{d\delta_{d,i}}{da} = (1 + w_d)\frac{d\delta_{m,i}}{da} + \frac{dw_d}{da}\delta_{m,i}. \quad (17)$$

According to the above argument, by fixing the initial condition of  $\phi_i$  we have all the initial conditions. We set  $\phi_i = -6 \times 10^{-7}$  which corresponds to  $\delta_m = 0.1$  at present time for  $k = 0.1h\text{Mpc}^{-1}$ . Our results are robust under small changes of the initial conditions, and we don't worry about the exact values. (For  $\phi_i = -7 \times 10^{-8}$ ,  $\delta_m$  reach to 0.01 at present time but  $f\sigma_8$  differs less than  $10^{-4}\%$ .)

DE clustering affects the growth of matter perturbations through the change of the potential  $\phi$ . As we noticed the amount of DE clustering is directly related to its effective sound speed. We restrict our analysis to the choice of  $k = 1/\lambda = 0.1h\text{Mpc}^{-1}$  which corresponds to  $\lambda = 10h^{-1}\text{Mpc}$  (Zhang et al. 2012). Note that the power-spectrum normalization  $\sigma_8$  which is the rms mass fluctuation on a scale  $R_8 = 8h^{-1}\text{Mpc}$  corresponds to  $k = 0.125h\text{Mpc}^{-1}$ . On the other hand it has been common practice to assume that the shape of the power spectrum recovered from galaxy surveys matches the linear matter power spectrum shape on scales  $k \leq 0.15h\text{Mpc}^{-1}$  (Smith et al. 2003; Tegmark et al. 2004; Percival et al. 2007). Obviously the choice of  $k = 0.1h\text{Mpc}^{-1}$  assures that we are in the linear regime. We find that small variations around this value do not really affect the qualitative evolution of the growth rate of clustering and thus of  $\gamma(z)$ .<sup>1</sup>

To compare these results with observations we calculate the growth factor  $f(z) = -\frac{1+z}{\delta_m(z)}\frac{d\delta_m(z)}{dz}$  and the growth index  $\gamma(z) = \frac{d \ln f(z)}{\Delta \Omega_m(z)}$  using our numerical results. The growth index in the  $\Lambda\text{CDM}$  model is redshift-independent and approximately equal to  $\gamma = 0.55$ . To compare this model to observational data we need to evaluate  $f(z)\sigma_8(z)$  where  $\sigma_8(z)$  is the mass variance in a sphere of radius of 8 Mpc/h. The variance  $\sigma_8(z)$  can be written in terms of  $\sigma_8$  at present time as  $\sigma_8(z) = \sigma_8(z=0)\frac{\delta_m(z)}{\delta_m(z=0)}$ . Also, in order to treat  $\sigma_8 \equiv \sigma_8(z=0)$  properly for the DE models we rescale the value of  $\sigma_8$  by  $\sigma_8 = \frac{\delta_m(z=0)}{\delta_{m,\Lambda}(z=0)}\sigma_{8,\Lambda}$ . Regarding  $\sigma_{8,\Lambda}$  we utilise  $\sigma_{8,\Lambda} = 0.818(0.30/\Omega_m)^{0.26}$  provided by the *Planck* analysis of Spergel et al. (2015) and it is also in agreement with the results of *Planck 2015* (Planck Collaboration XIII 2015).

DE perturbations not only depend on the sound speed but also on the EoS  $w_d$ . In the limit  $w_d \rightarrow -1$  all DE perturbations are washed out due to the  $1 + w_d$  factor in front of the source term in the evolution equation of  $\delta_d$ . To show how the DE sound speed affects the linear evolution of DM, we consider  $\Omega_m = 0.28$  and  $h = 0.7$  in the  $w\text{CDM}$  model to evaluate  $\delta_d$  and  $\Delta_d = \frac{\delta_d}{\delta_m}$ , the relative DE density contrast, for a few distinct values of the DE sound speed as a function of the EoS. In Fig. (1) the density contrast of DE as a function of  $w_d$  at the present time is presented. The non-clustering case remains homogeneous but for small values of the DE sound speed, the density contrast grows while increasing

<sup>1</sup> Since we are in the linear regime we verify that for different values of  $k$  the differences in  $f\sigma_8$  are practically negligible ( $\sim 10^{-5}\%$ ).

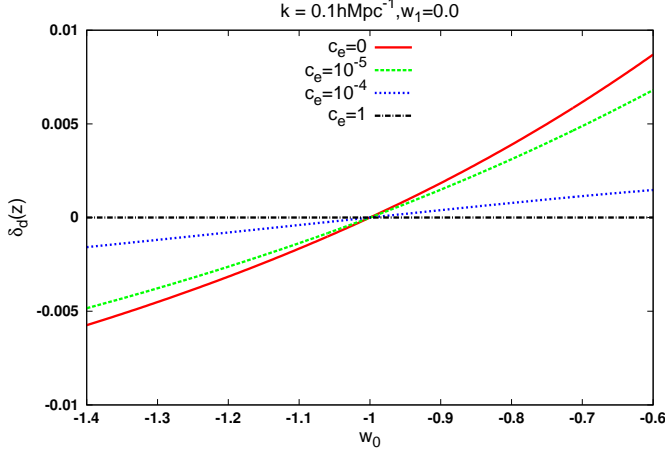


**Figure 1.** The density contrast of DE as a function of the EoS at the present time for four different values of the sound speed. The red solid curve shows a fully clustering DE model with  $c_e = 0$ . The green dashed (blue dotted) curve is for  $c_e = 10^{-5}$  ( $c_e = 10^{-4}$ ). A non-clustering model with  $c_e = 1$  is shown by a black dashed-dotted line.

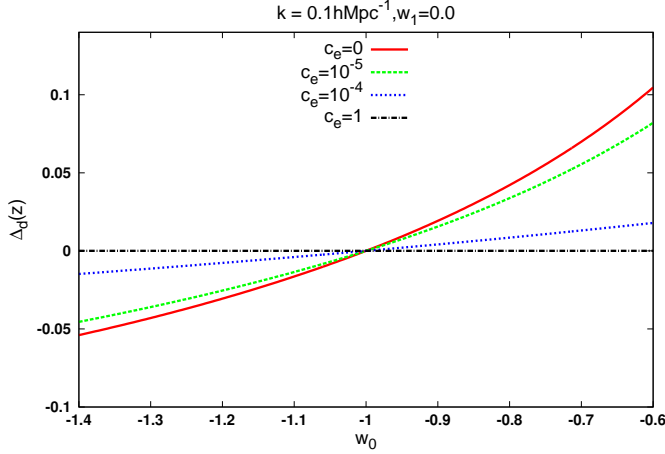


**Figure 2.** The relative density contrast of DE as a function of the EoS at the present time for four different values of the sound speed. Line style and colours are as in Fig. (1).

the EoS. In contrast to the non-clustering case, the fully clustering regime with  $c_e = 0$  gives a maximum value for the DE density contrast. In Fig. (2) the relative DE density contrast is shown as a function of EoS. The behaviour of this quantity is similar to that of the density contrast.

As we stated the quantity  $f\sigma_8(z)$  is affected by DE clustering. To show how  $f\sigma_8(z)$  changes with the DE sound speed, we evaluate  $\Delta f\sigma_8(z) = \frac{f_h\sigma_{s,h}(z) - f\sigma_8(z)}{f\sigma_8(z)} \times 100$  and  $\Delta\gamma(z) = \frac{\gamma_h(z) - \gamma(z)}{\gamma(z)} \times 100$  as a function of the EoS parameter. In the previous equations,  $h$  stands for homogeneous DE. For the growth rate, results at present time are presented in Fig. (3). As expected, the deviation increases by increasing the EoS and for  $w_d < -0.9$  the difference is less than 1%. The relative difference between homogeneous and clustering DE for the growth index  $\Delta\gamma(z=0)$  has been shown in Fig. (4). The difference between the homogeneous and the clustering DE models is also very small for  $w_d$  very close to the  $\Lambda$ CDM model.

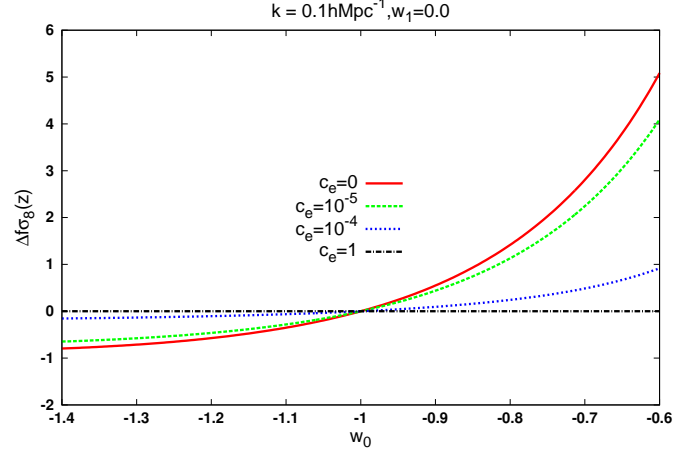


**Figure 3.** The relative difference of  $f\sigma_8$  at the present time as a function of EoS. Line style and colours are as in Fig. (1).

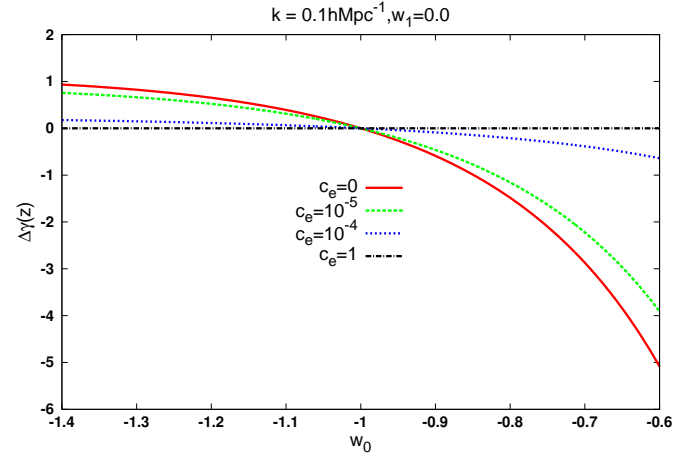


**Figure 4.** The relative difference of the growth index at present time as a function of EoS. Line style and colours are as in Fig. (1).

### 3 OBSERVATIONAL CONSTRAINTS ON THE DARK ENERGY SOUND SPEED

In this section we use current available observational data sets to constrain the cosmological background parameters and the DE sound speed. In this analysis we assume that the DE sound speed is constant in time, regardless of the particular equation-of-state parameter adopted. Our cosmological model will be described by the following parameters:  $\Omega_{m0}$  (matter density),  $\Omega_{b0}$  (baryon density),  $h = H_0/100$  (normalised Hubble constant),  $w_0$  and  $w_1$  (dark energy equation-of-state parameters) and  $c_e$  (effective sound speed) to describe the dark energy perturbations. In our analysis we assume a flat universe so that  $\Omega_{DM} + \Omega_b + \Omega_d = 1$ , hence the amount of dark energy is known from the knowledge of the matter and baryon density parameters.

The first data set we consider is the SnIa distance module from Union 2.1 sample (Suzuki et al. 2012). This data set includes 580 SnIa and its  $\chi^2$  is given by:

$$\chi_{\text{sn}}^2 = \sum_i \frac{[\mu_{\text{th}}(z_i) - \mu_{\text{ob}}(z_i)]^2}{\sigma_i^2}, \quad (18)$$

**Table 1.** The current available BAO data which we use in our analysis.

$z$	$d_i$	Survey & References
0.106	0.336	6dF (Beutler et al. 2011)
0.35	0.113	SDSS-DR7 (Padmanabhan et al. 2012)
0.57	0.073	SDSS-DR9 (Anderson et al. 2013)
0.44	0.0916	WiggleZ (Blake et al. 2011)
0.6	0.0726	WiggleZ (Blake et al. 2011)
0.73	0.0592	WiggleZ (Blake et al. 2011)

where  $\mu_{\text{th}}(z) = 5 \log_{10} \left[ (1+z) \int_0^z \frac{dx}{E(x)} \right] + \mu_0$ ,  $\mu_0 = 42.384 - 5 \log_{10} h$  and  $\sigma_i$  are the corresponding uncertainties. Before finding the minimum of  $\chi_{\text{sn}}^2$  we can expand  $\chi_{\text{sn}}^2$  around  $\mu_0$

$$\chi_{\text{sn}}^2 = A + 2B\mu_0 + C\mu_0^2, \quad (19)$$

where

$$A = \sum_i \frac{[\mu_{\text{th}}(\mu_0 = 0) - \mu_{\text{ob}}]^2}{\sigma_i^2},$$

$$B = \sum_i \frac{[\mu_{\text{th}}(\mu_0 = 0) - \mu_{\text{ob}}]}{\sigma_i^2},$$

$$C = \sum_i \frac{1}{\sigma_i^2}.$$

Obviously, for  $\mu_0 = -B/C$  Eq. (19) has a minimum, namely  $A - \frac{B^2}{C}$ . Now by defining  $\tilde{\chi}_{\text{sn}}^2 = A - \frac{B^2}{C}$ , we can use the minimum of  $\tilde{\chi}_{\text{sn}}^2$  which is independent of  $\mu_0$  in order to find the best values of the parameters. Of course both estimators provide the same results (Nesseris & Perivolaropoulos 2005).

The second data set we consider is the BAO sample which includes 6 distinct measurements of the baryon acoustic scale. These 6 data points and their references are summarised in Tab. (1).

To find the  $\chi_{\text{BAO}}^2$  we follow the same procedure as Hinshaw et al. (2013). So the  $\chi_{\text{BAO}}^2$  is given by

$$\chi_{\text{BAO}}^2 = \mathbf{Y}^T \mathbf{C}_{\text{BAO}}^{-1} \mathbf{Y}, \quad (20)$$

where  $\mathbf{Y} = (d(0.1) - d_1, \frac{1}{d(0.35)} - \frac{1}{d_2}, \frac{1}{d(0.57)} - \frac{1}{d_3}, d(0.44) - d_4, d(0.6) - d_5, d(0.73) - d_6)$  and

$$d(z) = \frac{r_s(z_{\text{drag}})}{D_V(z)}, \quad (21)$$

with

$$r_s(a) = \int_0^a \frac{c_s da}{a^2 H(a)}, \quad (22)$$

is the comoving sound horizon at the baryon drag epoch,  $c_s$  the baryon sound speed and  $D_V(z)$  is defined by:

$$D_V(z) = \left[ (1+z)^2 D_A^2(z) \frac{z}{H(z)} \right]^{\frac{1}{3}}, \quad (23)$$

and  $D_A(z)$  is the angular diameter distance. We used the fitting formula for  $z_d$  from Eisenstein & Hu (1998) and the baryon sound speed is given by:

$$c_s(a) = \frac{1}{\sqrt{3(1 + \frac{3\Omega_b^0}{4\Omega_m^0} a)}}, \quad (24)$$

where we set  $\Omega_\gamma^0 = 2.469 \times 10^{-5} h^{-2}$  (Hinshaw et al. 2013).

The covariance matrix  $\mathbf{C}_{\text{BAO}}^{-1}$  in Eq. (20) was obtained by Hinshaw et al. (2013)

$$\begin{pmatrix} 4444.4 & 0. & 0. & 0. & 0. & 0. \\ 0. & 34.602 & 0. & 0. & 0. & 0. \\ 0. & 0. & 20.6611 & 0. & 0. & 0. \\ 0. & 0. & 0. & 24532.1 & -25137.7 & 12099.1 \\ 0. & 0. & 0. & -25137.7 & 134598.4 & -64783.9 \\ 0. & 0. & 0. & 12099.1 & -64783.9 & 128837.6 \end{pmatrix}.$$

The position of the CMB acoustic peak provides a useful data to constrain dark energy models. The position of this peak is given by  $(l_a, R, z_*)$ , where  $R$  is the scale distance to recombination

$$l_a = \pi \frac{D_A(z_*)}{r_s(z_*)}, \quad (25)$$

$$R = \sqrt{\Omega_m^0} H_0 D_A(z_*), \quad (26)$$

and  $r_s(z)$  is the comoving sound horizon defined in Eq. (22). In this case we used the formula for  $z_*$  from Hu & Sugiyama (1996). For the WMAP data set we have (Hinshaw et al. 2013)

$$\mathbf{X}_{\text{CMB}} = \begin{pmatrix} l_a - 302.40 \\ R - 1.7264 \\ z_* - 1090.88 \end{pmatrix}, \quad (27)$$

and

$$\mathbf{C}_{\text{CMB}}^{-1} = \begin{pmatrix} 3.182 & 18.253 & -1.429 \\ 18.253 & 11887.879 & -193.808 \\ -1.429 & -193.808 & 4.556 \end{pmatrix}. \quad (28)$$

In addition to this data set the *Planck* data provide more accurate CMB data for which the position of the acoustic peak is given by (Shafer & Huterer 2014)

$$\mathbf{X}_{\text{CMB}} = \begin{pmatrix} l_a - 301.65 \\ R - 1.7499 \\ z_* - 1090.41 \end{pmatrix}, \quad (29)$$

and

$$\mathbf{C}_{\text{CMB}}^{-1} = \begin{pmatrix} 42.7044 & -418.36 & -0.7820 \\ -418.36 & 57366.3 & -762.152 \\ -0.7820 & -762.152 & 14.6995 \end{pmatrix}. \quad (30)$$

In both cases the  $\chi_{\text{CMB}}^2$  is given by:

$$\chi_{\text{CMB}}^2 = \mathbf{X}_{\text{CMB}}^T \mathbf{C}_{\text{CMB}}^{-1} \mathbf{X}_{\text{CMB}}. \quad (31)$$

A further data set used in this work is the Hubble evolution data obtained from the evolution of galaxies (Simon et al. 2005). We use the 12 available data points and the  $\chi^2$  for this data set is:

$$\chi_{\text{H}}^2 = \sum_i \frac{[H(z_i) - H_{\text{ob},i}]^2}{\sigma_i^2}. \quad (32)$$

The Big Bang Nucleosynthesis (BBN) provides a data point (Serra et al. 2009; Burles et al. 2001) which constrains mostly  $\Omega_b^0$ . The  $\chi_{\text{BBN}}^2$  is given by

$$\chi_{\text{BBN}}^2 = \frac{(\Omega_b^0 h^2 - 0.022)^2}{0.002^2}. \quad (33)$$

The final data set used is the growth rate data. These data were derived from redshift space distortions from galaxy surveys including PSCs, 2DF, VVDS, SDSS, 6dF, 2MASS, BOSS and WiggleZ and the data with their references are shown in Tab. 2. We solve Eqs. (10) and (11) numerically to find  $f(z)\sigma_8(z)$  and compute  $\chi_{\text{fs}}^2$  with

$$\chi_{\text{fs}}^2 = \sum_i \frac{[f\sigma_8(z_i) - f\sigma_{8,\text{ob}}]^2}{\sigma_i^2}. \quad (34)$$

**Table 2.** The  $f\sigma_8(z)$  data points including their references and surveys.

$z$	$f\sigma_8(z)$	Reference
0.02	$0.360 \pm 0.040$	Hudson & Turnbull (2013)
0.067	$0.423 \pm 0.055$	Beutler et al. (2012)
0.10	$0.37 \pm 0.13$	Feix et al. (2015)
0.17	$0.510 \pm 0.060$	Percival et al. (2004)
0.35	$0.440 \pm 0.050$	Song & Percival (2009); Tegmark et al. (2006)
0.77	$0.490 \pm 0.180$	Guzzo et al. (2008); Song & Percival (2009)
0.25	$0.351 \pm 0.058$	Samushia et al. (2012)
0.37	$0.460 \pm 0.038$	Samushia et al. (2012)
0.22	$0.420 \pm 0.070$	Blake et al. (2011)
0.41	$0.450 \pm 0.040$	Blake et al. (2011)
0.60	$0.430 \pm 0.040$	Blake et al. (2011)
0.60	$0.433 \pm 0.067$	Tojeiro et al. (2012)
0.78	$0.380 \pm 0.040$	Blake et al. (2011)
0.57	$0.427 \pm 0.066$	Reid et al. (2012)
0.30	$0.407 \pm 0.055$	Tojeiro et al. (2012)
0.40	$0.419 \pm 0.041$	Tojeiro et al. (2012)
0.50	$0.427 \pm 0.043$	Tojeiro et al. (2012)
0.80	$0.47 \pm 0.08$	de la Torre et al. (2013)

**Table 3.** The best value parameters and their  $1-\sigma$  uncertainty for the wCDM model.

Parameters	Best (WMAP)	Best (Planck)
$h$	$0.6955^{+0.0040}_{-0.0037}$	$0.7064^{+0.0011}_{-0.0012}$
$\Omega_{\text{DM}}^0$	$0.2273^{+0.0027}_{-0.0029}$	$0.2361^{+0.0010}_{-0.0010}$
$\Omega_{\text{b}}^0$	$0.0470^{+0.0004}_{-0.0005}$	$0.0482^{+0.0003}_{-0.0002}$
$w_0$	$-0.9436^{+0.0144}_{-0.0141}$	$-0.9975^{+0.0055}_{-0.0053}$
$c_e$	0.	0.001
$\sigma_8$	0.837	0.829

The overall likelihood function is given by the product of the individual likelihoods:

$$\mathcal{L}_{\text{tot}} = \mathcal{L}_{\text{sn}} \times \mathcal{L}_{\text{BAO}} \times \mathcal{L}_{\text{CMB}} \times \mathcal{L}_H \times \mathcal{L}_{\text{BBN}} \times \mathcal{L}_{\text{fs}}, \quad (35)$$

and the total chi-square  $\chi_{\text{tot}}^2$  is given by:

$$\chi_{\text{tot}}^2 = \chi_{\text{sn}}^2 + \chi_{\text{BAO}}^2 + \chi_{\text{CMB}}^2 + \chi_H^2 + \chi_{\text{BBN}}^2 + \chi_{\text{fs}}^2. \quad (36)$$

We calculate the total chi-square  $\chi_{\text{tot}}^2$  and find the best value of the parameters with an MCMC algorithm. The number of degrees of freedom is  $\nu = N - n_{\text{fit}} - 1$ , where  $N = 616$  and  $n_{\text{fit}}$  is the number of the fitted parameters. The results of this analysis for the wCDM, w(t)CDM and  $\Lambda$ CDM are summarized in Tabs. (3), (4) and (5) respectively.

To compare the DE models we have computed the corrected Akaike information criterion (AIC) (Akaike 1974; Sugiura 1978) which, in our case, due to  $N/n_{\text{fit}} > 40$ , is given by:

$$\text{AIC} = \chi_{\text{min}}^2 + 2n_{\text{fit}}. \quad (37)$$

A smaller value of AIC indicates a better model-data fit. Of course it is well known that small differences in AIC are not necessarily significant and therefore, in order to assess the effectiveness of the different models in reproducing the data, we need to estimate the

**Table 4.** The best value parameters and their  $1-\sigma$  uncertainty for the w(t)CDM model.

Parameters	Best (WMAP)	Best (Planck)
$h$	$0.7001^{+0.0040}_{-0.0038}$	$0.7070^{+0.0012}_{-0.0013}$
$\Omega_{\text{DM}}^0$	$0.2234^{+0.0028}_{-0.0027}$	$0.2361^{+0.0012}_{-0.0011}$
$\Omega_{\text{b}}^0$	$0.0474^{+0.0005}_{-0.0005}$	$0.0481^{+0.0003}_{-0.0003}$
$w_0$	$-1.0176^{+0.0128}_{-0.0124}$	$-0.95204^{+0.0060}_{-0.0058}$
$w_1$	$0.3289^{+0.0395}_{-0.0405}$	$-0.18512^{+0.0205}_{-0.0195}$
$c_e$	0.002	0.
$\sigma_8$	0.840	0.829

**Table 5.** The best value parameters and their  $1-\sigma$  uncertainty for the  $\Lambda$ CDM model.

Parameters	Best (WMAP)	Best (Planck)
$h$	$0.7048^{+0.0042}_{-0.0041}$	$0.7069^{+0.0011}_{-0.0010}$
$\Omega_{\text{DM}}^0$	$0.2261^{+0.0030}_{-0.0029}$	$0.2359^{+0.0010}_{-0.0011}$
$\Omega_{\text{b}}^0$	$0.0456^{+0.0006}_{-0.0005}$	$0.0481^{+0.0003}_{-0.0003}$
$\sigma_8$	0.839	0.829

model pair difference  $\Delta\text{AIC} = \text{AIC}_y - \text{AIC}_x$ . The higher the value of  $|\Delta\text{AIC}|$ , the higher the evidence against the model with a higher value of AIC. With a difference  $|\Delta\text{AIC}| \geq 2$  indicating a positive evidence and  $|\Delta\text{AIC}| \geq 6$  indicating a strong evidence, while a value  $|\Delta\text{AIC}| \leq 2$  indicates consistency among the two models. The results of our analysis are the following:

(i) Using WMAP data:

- For the wCDM model,  $\chi_{\text{min}}^2 = 586.53$ ,  $n_{\text{fit}} = 5$ , so  $\text{AIC}=596.53$
- For the w(t)CDM model,  $\chi_{\text{min}}^2 = 585.32$ ,  $n_{\text{fit}} = 6$ , so  $\text{AIC}=597.32$
- For the  $\Lambda$ CDM model,  $\chi_{\text{min}}^2 = 589.22$ ,  $n_{\text{fit}} = 3$ , so  $\text{AIC}=595.32$

(ii) Using Planck data:

- For the wCDM model,  $\chi_{\text{min}}^2 = 595.76$ ,  $n_{\text{fit}} = 5$ , so  $\text{AIC}=605.76$
- For the w(t)CDM model,  $\chi_{\text{min}}^2 = 595.50$ ,  $n_{\text{fit}} = 6$ , so  $\text{AIC}=607.50$
- For the  $\Lambda$ CDM model,  $\chi_{\text{min}}^2 = 595.79$ ,  $n_{\text{fit}} = 3$ , so  $\text{AIC}=601.79$

Concerning the best value of the dark energy sound speed we find that it tends to zero but the corresponding error bars remain quite large within  $1\sigma$ . In particular  $c_e$  lies in the range  $\in [0, 1]$ .

In order to investigate the range of validity for  $c_e$ , in Figs. (5) and (6) we provide the  $1\sigma$  and  $2\sigma$  contours of our analysis. Note that in both plots the upper panels are for wCDM in which we present the confidence levels in the  $(c_e, \Omega_m)$  and  $(c_e, w)$  planes, where  $\Omega_m = \Omega_{\text{DM}}^0 + \Omega_{\text{b}}^0$ . In the bottom panels of Figs. (5) and

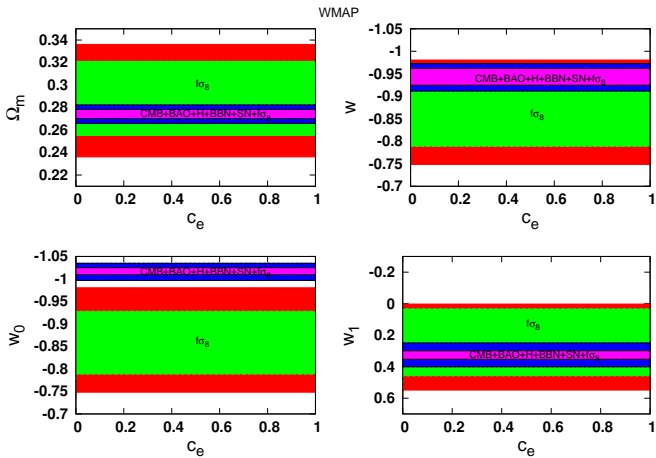


**Figure 5.** The  $1\sigma$  and  $2\sigma$  contours of  $\Omega_m(w\text{CDM})$ ,  $w(w\text{CDM})$ ,  $w_0(w(t)\text{CDM})$  and  $w_1(w(t)\text{CDM})$  versus DE sound speed using *WMAP* data. The  $1\sigma$  and  $2\sigma$  contours correspond to  $\chi^2 - \chi_b^2 = 2.3$  and  $\chi^2 - \chi_b^2 = 6.16$ . The green (red) area correspond to  $1\sigma$  ( $2\sigma$ ) using only  $f\sigma_8$  data and purple (blue) show  $1\sigma$  ( $2\sigma$ ) using all data set.

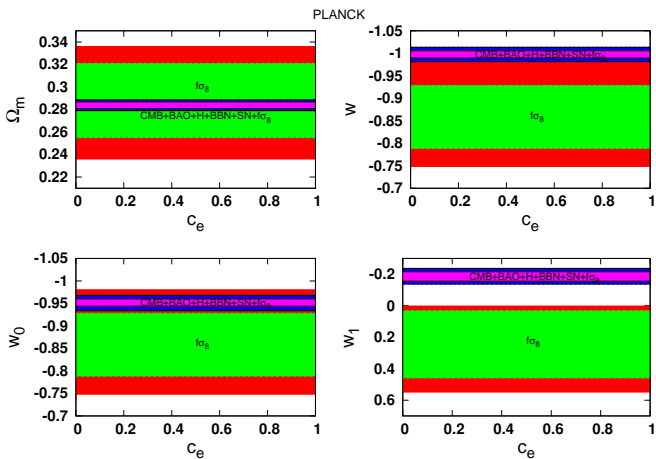


**Figure 6.** Same as Fig. (5) but using the *Planck* shift parameter.

(6) the contours for  $w_0$  and  $w_1$  in the CPL model are shown with respect to the DE sound speed. From this analysis it becomes clear that there is a strong degeneracy between  $c_e$  and  $(\Omega_m, w)$  which implies that all values in the interval  $0 \leq c_e \leq 1$  are acceptable within the  $1\sigma$  uncertainty. As we stated, with data used in this paper the error bar of DE sound speed is quite large.

In Figs. (7) and (8) we present the quantity  $f\sigma_8(z)$  for our best value parameters by considering the *Planck* and *WMAP* data for the  $w\text{CDM}$ ,  $w(t)\text{CDM}$  and the  $\Lambda\text{CDM}$  models, respectively. We also show the observational data points. In addition to this quantity in Figs. (9) and (10) the growth index for the best values of the parameters have been shown. Note that using *Planck* CMB data our likelihood analysis indicates that all three models are very close to each others.<sup>2</sup>

Previous works in literature tried to put constraints on the dark energy effective sound speed  $c_e$  using different kind of data. de Putter et al. (2010) combination of CMB temperature power

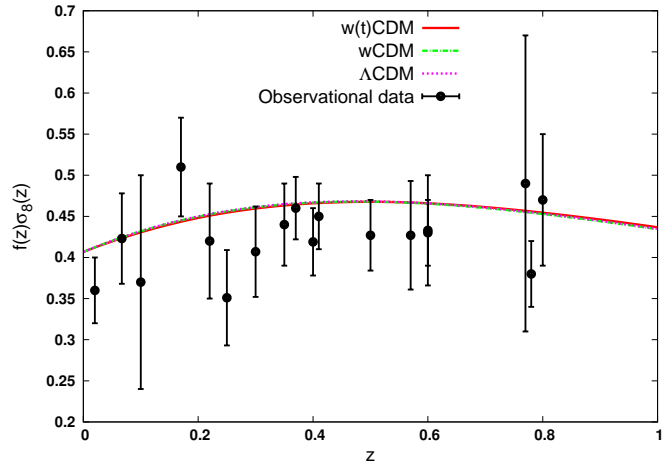


**Figure 7.** The  $f\sigma_8(z)$  quantity (using *Planck* data), for the best values cosmological parameters for the  $w\text{CDM}$  (green dot-dashed curve) and  $w(t)\text{CDM}$  (red solid curve) models. The  $\Lambda\text{CDM}$  model is shown by the violet short-dashed curve.

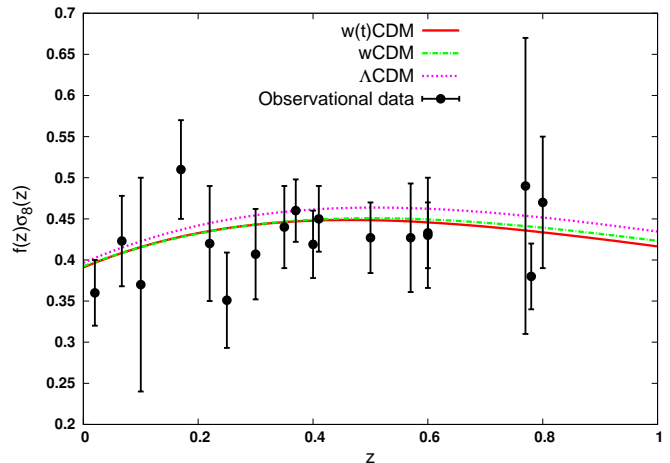


**Figure 8.** The  $f\sigma_8(z)$  quantity (using *WMAP* data), for the best values cosmological parameters for the  $w\text{CDM}$  (green dot-dashed curve) and  $w(t)\text{CDM}$  (red solid curve) models. The  $\Lambda\text{CDM}$  model is shown by the violet short-dashed curve.

spectrum data, their cross-correlation with several mass-density tracers and the SDSS LRG auto-correlation function. Supernovae data were used to break degeneracies with background cosmological parameters. Hannestad (2005) set of Supernova data, LSS and CMB power spectra. Finally Xia et al. (2008) performed a similar analysis for a single perfect fluid and a two-field Quintom dark energy model with  $w = -1$  crossing by analysing CMB anisotropy data, LSS and SNIa observational data. In all these studies, using a similar approach to the one used in this work, the authors reach our same results. While previous and current data can constrain at a good level the current equation-of-state parameter of the dark energy component, the quality of the observations is unfortunately still not sufficient enough to put any constraint on the dark energy effective sound speed. Note however that this is also due to the negligible contribution of dark energy at early times on one side, and to the fact that current observations favour  $w \simeq -1$ . As pointed out by de Putter et al. (2010), if one considers the case of early dark energy models (Doran & Robbers 2006) where the contribution of

<sup>2</sup> See the results of  $\chi^2$  for the *Planck* case.

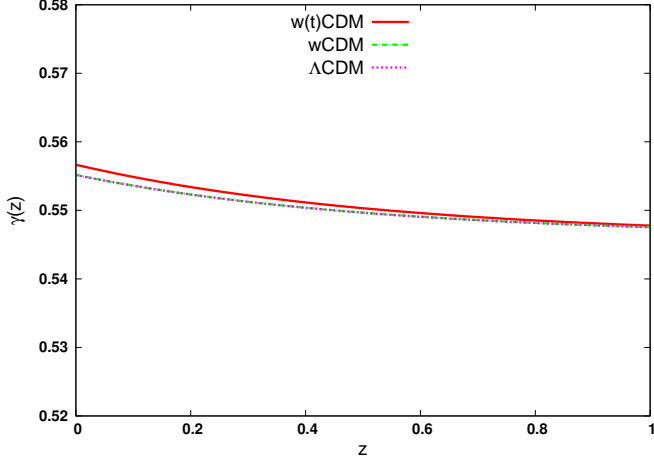


**Figure 9.** The growth index (using *Planck* data), for the best values cosmological parameters for the wCDM (green dot-dashed curve) and w(t)CDM (red solid curve) models. The  $\Lambda$ CDM model is shown by the violet short-dashed curve.

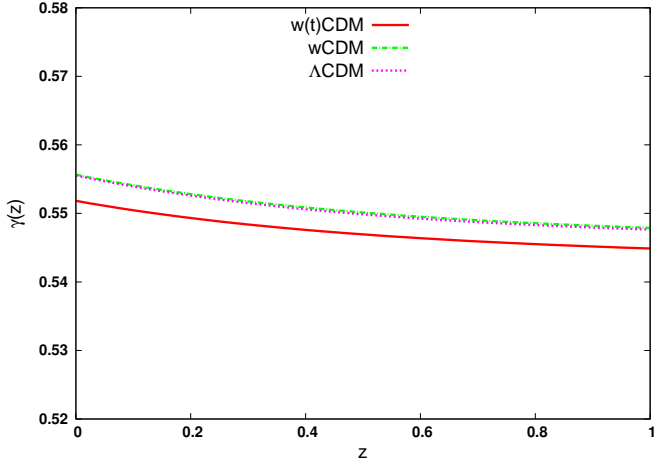


**Figure 10.** The growth index (using *WMAP* data), for the best values cosmological parameters for the wCDM (green dot-dashed curve) and w(t)CDM (red solid curve) models. The  $\Lambda$ CDM model is shown by the violet short-dashed curve.

dark energy at early times, i.e. CB, is not negligible, then more stringent limits can be set on  $c_e$ .

#### 4 GROWTH INDEX ANALYTIC SOLUTION

In section 2 we investigated the evolution of the growth index by solving numerically the system of Eqs. (5), (10) and (11). Here our aim is to extend the work of Basilakos (2015) in order to provide a general  $\gamma(z)$  approximated solution which can be used in studies of structure formation. On sub-horizon scales, namely  $\frac{k^2}{a^2} \gg H^2$  (or  $k^2 \gg \mathcal{H}^2$ ), Poisson equation (see appendix B) takes the form

$$-\frac{k^2}{a^2}\phi = \frac{3H^2}{2} [\Omega_m \delta_m + \Omega_d \delta_d (1 + 3c_e)] . \quad (38)$$

Under the above conditions, Eq. (10) becomes

$$a^2 \frac{d^2 \delta_m}{da^2} + a \left( 3 + \frac{\dot{H}}{H^2} \right) \frac{d\delta_m}{da} = \frac{3}{2} [\Omega_m \delta_m + (1 + 3c_e) \Omega_d \delta_d] .$$

(39)

In this framework, for  $\delta_d = 0$ , the latter equation reduces to the well known scale independent equation which is also valid for the concordance  $\Lambda$  cosmology.

Concerning the equation of state parameter, it is well known that one can express it in terms of the Hubble parameter (Saini et al. 2000; Huterer & Turner 2001)

$$w_d(a) = \frac{-1 - \frac{2}{3} a \frac{d \ln H}{da}}{1 - \Omega_m(a)} , \quad (40)$$

or

$$a \frac{d \ln H}{da} = \frac{\dot{H}}{H^2} = -\frac{3}{2} - \frac{3}{2} w_d(a) \Omega_d(a) , \quad (41)$$

where  $\Omega_m(a) = 1 - \Omega_d(a) = \frac{\Omega_{m0}}{a^3 E^2(a)}$  and  $E(a) = H(a)/H_0$ . Now, substituting Eq. (41) and  $f = d \ln \delta_m / d \ln a$  into Eq. (39) we obtain the basic differential equation which governs the growth rate of clustering

$$a \frac{df}{da} + f^2 + \left( \frac{1}{2} - \frac{3}{2} w_d \Omega_d \right) f = \frac{3}{2} [\Omega_m + (1 + 3c_e) \Delta_d \Omega_d] , \quad (42)$$

where  $\Delta_d(a) \equiv \delta_d / \delta_m$ . To this end, changing the variables in Eq. (42) from  $a(z)$  to redshift [ $\frac{df}{da} = -(1+z)^{-2} \frac{df}{dz}$ ] and utilising  $f(z) = \Omega_m(z)^{\gamma(z)}$  we arrive to

$$-(1+z)\gamma_z \ln(\Omega_m) + \Omega_m^\gamma + 3w_d \Omega_d \left( \gamma - \frac{1}{2} \right) + \frac{1}{2} = \frac{3}{2} \Omega_m^{1-\gamma} X , \quad (43)$$

where  $\gamma_z = d\gamma/dz$  and

$$X(z) = 1 + \frac{\Omega_d(z)}{\Omega_m(z)} \Delta_d(z) (1 + 3c_e) . \quad (44)$$

On the other hand, the parametrization  $f(a) = d \ln \delta_m / d \ln a \simeq \Omega_m(a)^{\gamma(a)}$  has a great impact in cosmological studies because it can be used in order to simplify the numerical calculations of Eq. (39). Obviously, a direct integration gives

$$\delta_m(a, \gamma) = a(z) \exp \left[ \int_{a_i}^{a(z)} \frac{du}{u} (\Omega_m^\gamma(u) - 1) \right] , \quad (45)$$

where  $a(z) = 1/(1+z)$  and  $a_i$  is the scale factor of the universe at which the matter component dominates the cosmic fluid (here we use  $a_i \simeq 10^{-1}$  or  $z_i \simeq 10$ ). Hence, the linear growth factor normalised to unity at the present epoch is  $D(a) = \frac{\delta_m(a, \gamma)}{\delta_m(1, \gamma)}$ . Therefore, in order to proceed with the analysis we need to somehow know the functional form of  $\gamma(z)$ . From the phenomenological point of view we may parametrize  $\gamma(z)$  as follows

$$\gamma(z) = \gamma_0 + \gamma_1 y(z) . \quad (46)$$

This equation can be seen as a first order Taylor expansion around some cosmological quantity such as  $a(z)$  and  $z$ .

Recently, it has been found (Basilakos 2012; Basilakos & Pouri 2012, and references therein) that for those  $y(z)$  functions which satisfy the condition  $y(0) = 0$  [or  $\gamma(0) = \gamma_0$ ], the parameter  $\gamma_1$  is written as a function of  $\gamma_0$ . For example, at the present epoch [ $z = 0$ ,  $\gamma_z(0) = \gamma_1 y_z(0)$ ,  $X_0 = X(0)$ ,  $w_0 = w_d(0)$ ], Eq. (43) is written as

$$\gamma_1 = \frac{\Omega_{m0}^{\gamma_0} + 3w_0(\gamma_0 - \frac{1}{2})\Omega_{d0} + \frac{1}{2} - \frac{3}{2}\Omega_{m0}^{1-\gamma_0} X_0}{y_z(0) \ln \Omega_{m0}} , \quad (47)$$

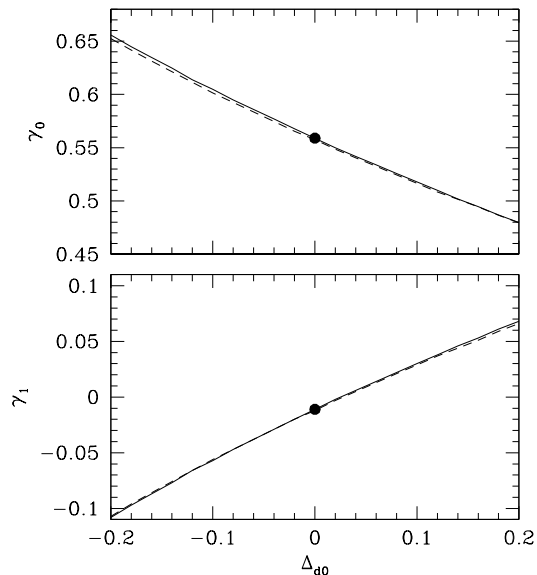


**Figure 11.** The pair  $(\gamma_0, \gamma_1)$  as a function of  $\Delta_{d0}$ . The solid and the dashed lines correspond to the  $w(t)$ CDM and  $w$ CDM dark energy models, respectively. The homogeneous case  $\Delta_{d0} = 0$  is shown by the solid point. For the cosmological parameters, we use the values of Table 3 and 4 (third column).

where  $y_z = dy/dz$ . Note that a similar equation has been found in Basilakos (2015) in the case of  $c_e \equiv w_d$  with  $w_d = const$ . As it is expected, for the homogeneous DE case ( $\Delta_d = 0$ ,  $X = 1$ ), we verify that the above formula boils down to that of Polarski & Gannouji (2008) for  $y(z) = z$ . Within this framework, assuming  $y(z) = 1 - a(z) = \frac{z}{1+z}$  (Ballesteros & Riotto 2008), we fully recover results in literature (Ishak & Dossett 2009; Bueno Belloso et al. 2011; di Porto et al. 2012). Notice that below we focus on  $y(z) = 1 - a(z) = \frac{z}{1+z}$  with  $y_z(0) = 1$ . The fact that  $\Omega_d(z) \simeq 0$  at  $z \gg 1$  implies that the asymptotic value of the growth index  $\gamma_\infty = \gamma_0 + \gamma_1$  is not really affected by the dark energy clustering. Therefore, plugging  $\gamma_0 = \gamma_\infty - \gamma_1$ <sup>3</sup> into Eq. (47) we can obtain the constants  $\gamma_{0,1}$  in terms of  $(\Omega_{m0}, w_0, \Delta_{d0}, c_e)$ .

In Fig. (11) we present  $(\gamma_0, \gamma_1)$  as a function of  $\Delta_{d0}$ . The curves are constructed using the parameters from Table 3 and 4 (third column) and they correspond to  $w(t)$ CDM (solid) and  $w$ CDM (dashed) models. We observe that for  $\Delta_{d0} > 0$  the growth index starts to deviate from that of the  $\Lambda$ CDM model, namely  $\gamma_0 < 0.55$  and  $\gamma_1 > 0$ . In the case of  $\Delta_{d0} < 0$  the value of  $\gamma_0$  is greater than that of the homogeneous case ( $\gamma_0 > 0.55$ ). In this context, concerning the value of  $\gamma_1$  we find that it becomes negative. Of course for  $\Delta_{d0} = 0$  the pair  $(\gamma_0, \gamma_1)$  reduces to that of the homogeneous case (see solid points in Fig. (11)), as it should.

## 5 CONCLUSIONS

To summarize, we study the impact of dark energy clustering on the growth index of matter fluctuations. Initially we provide the most general form of the equations governing dark matter and dark

energy clustering within the framework of  $c_e = const$ . Then using the well known equation of state parameters, namely  $w_d(z) = w_0 + w_1 z/(1+z)$ ,  $w_d(z) = const$  and the current cosmological data we place constraints on the cosmological parameters, including that of the effective sound speed  $c_e$ . Although the likelihood function peaks at  $c_e \sim 0$ , which indicates that the dark energy component clusters in analogy to the matter component  $c_e \sim 0$ , the corresponding error bars are quite large within  $1 - \sigma$  uncertainties which implies that  $c_e$  remains practically unconstrained. We also compared our findings with previous work reaching the same conclusion that at the moment the quality of cosmological data is not sufficient enough to put constraint on the dark energy effective sound speed. Future cosmological data, based for example on *Euclid*, are expected to improve even further the relevant constraints on  $c_e$  and thus the validity of clustered dark energy will be effectively tested. Finally, we have derived a new approximated solution of the growth index in terms of the cosmological parameters, dark energy perturbations and  $c_e$ .

## ACKNOWLEDGEMENTS

We thank the anonymous referee whose comments helped to improve the paper.

## References

- Abramo L., Batista R., Liberato L., Rosenfeld R., 2009, Phys. Rev. D, 79, 023516
- Akaike H., 1974, IEEE Transactions of Automatic Control, 19, 716
- Akhoury R., Garfinkle D., Saotome R., 2011, JHEP, 1104, 096
- Amendola L., Tsujikawa S., 2010, Dark Energy: Theory and Observations. Cambridge University Press, Cambridge UK
- Anderson L., Aubourg E., Bailey S., Bizyaev D., Blanton M., et al., 2013, MNRAS, 427, 3435
- Armendariz-Picon C., Damour T., Mukhanov V. F., 1999, Phys. Lett. B, 458, 209
- Armendariz-Picon C., Mukhanov V. F., Steinhardt P. J., 2000, Phys. Rev. Lett., 85, 4438
- Astier P., et al., 2006, A&A, 447, 31
- Babichev E., Mukhanov V. F., Vikman A., 2006, JHEP, 0609, 061
- Ballesteros G., Riotto A., 2008, Phys. Lett. B, 668, 171
- Basilakos S., 2012, International Journal of Modern Physics D, 21, 50064
- Basilakos S., 2015, Mon. Not. Roy. Astron. Soc., 449, 2151
- Basilakos S., Bueno Sanchez J., Perivolaropoulos L., 2009, Phys. Rev. D, 80, 043530
- Basilakos S., Pouri A., 2012, Mon. Not. Roy. Astron. Soc., 423, 3761
- Basse T., Bjaelde O. E., Hamann J., Hannestad S., Wong Y. Y., 2014, JCAP, 1405, 021
- Batista R., Pace F., 2013, JCAP, 1306, 044
- Batista R. C., 2014, Phys. Rev. D, 89, 123508
- Bean R., Doré O., 2004, Phys. Rev. D, 69, 083503
- Bennett C., et al., 2003, ApJS, 148, 1
- Beutler F., Blake C., Colless M., Jones D. H., Staveley-Smith L., et al., 2011, MNRAS, 416, 3017
- Beutler F., Blake C., Colless M., Jones D. H., Staveley-Smith L., et al., 2012, MNRAS, 423, 3430
- Blake C., Brough S., Colless M., Contreras C., Couch W., et al., 2011, MNRAS, 415, 2876
- Blake C., Kazin E., Beutler F., Davis T., Parkinson D., et al., 2011, MNRAS, 418, 1707
- Bueno Belloso A., García-Bellido J., Sapone D., 2011, JCAP, 10, 10
- Burles S., Nollett K. M., Turner M. S., 2001, ApJ, 552, L1
- Capozziello S., Carloni S., Troisi A., 2003, Recent Res. Dev. Astron. Astrophys., 1, 625

<sup>3</sup> Regarding the asymptotic value of the growth index we use  $\gamma_\infty \approx 3(w-1)/(6w-5)$  for the  $w$ CDM model (see Linder & Cahn 2007; Nesseris & Perivolaropoulos 2008) and  $\gamma_\infty \approx 0.55 + 0.05[1 + w(z=1)]$  for the  $w(t)$ CDM model (Linder 2005).

Carroll S. M., Duvvuri V., Trodden M., Turner M. S., 2004, *Phys. Rev. D*, 70, 043528

Chevallier M., Polarski D., 2001, *IJMP D*, 10, 213

Chiba T., Dutta S., Scherrer R. J., 2009, *Phys. Rev. D*, 80, 043517

Chiba T., Okabe T., Yamaguchi M., 2000, *Phys. Rev. D*, 62, 023511

Cole S., et al., 2005, *MNRAS*, 362, 505

Copeland E. J., Sami M., Tsujikawa S., 2006, *IJMP D*, 15, 1753

de la Torre S., Guzzo L., Peacock J., Branchini E., Iovino A., et al., 2013, *A&A*, 557, A54

de Putter R., Huterer D., Linder E. V., 2010, *Phys. Rev. D*, 81, 103513

di Porto C., Amendola L., Branchini E., 2012, *MNRAS*, 419, 985

Dobado A., Maroto A. L., 1995, *Phys. Rev. D*, 52, 1895

Doran M., Robbers G., 2006, *JCAP*, 0606, 026

Dossett J., Ishak M., 2013, *Phys. Rev. D*, D88, 103008

Dvali G., Gabadadze G., Porrati M., 2000, *Phys. Lett. B*, 485, 208

Eisenstein D. J., et al., 2005, *ApJ*, 633, 560

Eisenstein D. J., Hu W., 1998, *ApJ*, 496, 605

Erickson J. K., Caldwell R., Steinhart P. J., Armendariz-Picon C., Mukhanov V. F., 2002, *Phys. Rev. Lett.*, 88, 121301

Feix M., Nusser A., Branchini E., 2015, *ArXiv e-prints*, 1503.05945

Garriga J., Mukhanov V. F., 1999, *Phys. Lett. B*, 458, 219

Guzzo L., Pierleoni M., Meneux B., Branchini E., Fevre O. L., et al., 2008, *Nature*, 451, 541

Hannestad S., 2005, *Phys. Rev.*, D71, 103519

Hawkins E., Maddox S., Cole S., Madgwick D., Norberg P., et al., 2003, *MNRAS*, 346, 78

Hinshaw G., et al., 2013, *ApJS*, 208, 19

Hu W., 1998, *ApJ*, 506, 485

Hu W., Scranton R., 2004, *Phys. Rev. D*, 70, 123002

Hu W., Sugiyama N., 1996, *ApJ*, 471, 542

Hudson M. J., Turnbull S. J., 2013, *ApJ*, 751, L30

Huterer D., Linder E. V., 2007, *Phys. Rev. D*, 75, 023519

Huterer D., Turner M. S., 2001, *Phys. Rev. D*, 64, 123527

Ishak M., Dossett J., 2009, *Phys. Rev. D*, 80, 043004

Jha S., Riess A. G., Kirshner R. P., 2007, *ApJ*, 659, 122

Kodama H., Sasaki M., 1984, *Prog. Theor. Phys. Suppl.*, 78, 1

Lima J., Zanchin V., Brandenberger R. H., 1997, *MNRAS*, 291, L1

Linder E. V., 2003, *Phys. Rev. Lett.*, 90, 091301

Linder E. V., 2005, *Phys. Rev. D*, 72, 043529

Linder E. V., Cahn R. N., 2007, *Astroparticle Physics*, 28, 481

Ma C.-P., Bertschinger E., 1995, *ApJ*, 455, 7

Magnano G., Sokolowski L. M., 1994, *Phys. Rev. D*, 50, 5039

Mehrabi A., Malekjani M., Pace F., 2015, *Astrophys. Space Sci.*, 356, 129

Nesseris S., Perivolaropoulos L., 2005, *Phys. Rev. D*, 72, 123519

Nesseris S., Perivolaropoulos L., 2008, *Phys. Rev. D*, 77, 023504

Nesseris S., Sapone D., 2014, *ArXiv e-prints*, 1409.3697

Pace F., Batista R. C., Del Popolo A., 2014, *MNRAS*, 445, 648

Padmanabhan N., Xu X., Eisenstein D. J., Scalzo R., Cuesta A. J., et al., 2012, *MNRAS*, 427, 2132

Peebles P., Ratra B., 2003, *Rev. Mod. Phys.*, 75, 559

Peebles P. J. E., 1993, *Principles of physical cosmology*. Princeton University Press

Percival W. J., et al., 2004, *MNRAS*, 353, 1201

Percival W. J., et al., 2007, *ApJ*, 657, 645

Perlmutter S., et al., 1997, *ApJ*, 483, 565

Perlmutter S., et al., 1998, *Nature*, 391, 51

Perlmutter S., et al., 1999, *ApJ*, 517, 565

Planck Collaboration XIII 2015, *ArXiv e-prints*, 1502.01589

Planck Collaboration XIV 2015, *ArXiv e-prints*, 1502.01590

Polarski D., Gannouji R., 2008, *Physics Letters B*, 660, 439

Rapetti D., Blake C., Allen S. W., Mantz A., Parkinson D., et al., 2013, *MNRAS*, 432, 973

Reid B. A., Samushia L., White M., Percival W. J., Manera M., et al., 2012, *MNRAS*, 426, 2719

Riess A. G., et al., 2004, *ApJ*, 607, 665

Sahni V., Starobinsky A. A., 2000, *IJMPD*, 9, 373

Saini T. D., Raychaudhury S., Sahni V., Starobinsky A. A., 2000, *Physical Review Letters*, 85, 1162

Samushia L., Percival W. J., Raccanelli A., 2012, *MNRAS*, 420, 2102

Sapone D., Majerotto E., 2012, *Phys. Rev. D*, 85, 123529

Schmidt H.-J., 1990, *Astron. Nachr.*, 311, 165

Seo H.-J., Eisenstein D. J., 2005, *ApJ*, 633, 575

Serra P., Cooray A., Holz D. E., Melchiorri A., Pandolfi S., et al., 2009, *Phys. Rev. D*, 80, 121302

Shafer D. L., Huterer D., 2014, *Phys. Rev. D*, 89, 063510

Simon J., Verde L., Jimenez R., 2005, *Phys. Rev. D*, 71, 123001

Smith R. E., et al., 2003, *MNRAS*, 341, 1311

Song Y.-S., Percival W. J., 2009, *JCAP*, 0910, 004

Spergel D., et al., 2003, *ApJS*, 148, 175

Spergel D., et al., 2007, *ApJS*, 170, 377

Spergel D. N., Flauger R., HloÅek R., 2015, *Phys. Rev. D*, 91, 023518

Steigerwald H., Bel J., Marinoni C., 2014, *JCAP*, 1405, 042

Sugiura N., 1978, *Communications in Statistics A, Theory and Methods*, 7, 13

Suzuki N., Rubin D., Lidman C., Aldering G., et al 2012, *ApJ*, 746, 85

Tegmark M., et al., 2004, *Phys. Rev. D*, 69, 103501

Tegmark M., et al., 2006, *Phys. Rev. D*, 74, 123507

Tojeiro R., Percival W., Brinkmann J., Brownstein J., Eisenstein D., et al., 2012, *MNRAS*, 424, 2339

Weinberg S., 1989, *Reviews of Modern Physics*, 61, 1

Xia J.-Q., Cai Y.-F., Qiu T.-T., Zhao G.-B., Zhang X., 2008, *Int. J. Mod. Phys.*, D17, 1229

Zhang W.-S., et al., 2012, *Sci China-Phys Mech Astron*, 55, 2244

## APPENDIX A: PROOF OF EQ. (12)

We start with Eqs. (6) and (7). The term  $\frac{\delta p}{\delta \rho}$  appears in both equations but it behaves very differently in these equations. In the first equation we have

$$-3\mathcal{H}\frac{\delta p}{\delta \rho}\delta = -3\mathcal{H}c_e\delta - 9\frac{\mathcal{H}^2}{k^2}(1+w_d)(c_e - c_a)\theta, \quad (\text{A1})$$

and on sub-horizon scale we can neglect the latter term ( $k^2 \gg \mathcal{H}^2$ ), but in Eq. (7) we have

$$k^2\frac{\delta p}{\delta \rho}\delta = k^2c_e\delta + 3\mathcal{H}(1+w_d)(c_e - c_a)\theta, \quad (\text{A2})$$

where the latter term can not be neglected. Differentiating Eq. (6) with respect to conformal time we have:

$$\begin{aligned} \delta'' &+ w'_d\theta + (1+w_d)\theta' + 3\mathcal{H}'c_e\delta \\ &+ 3\mathcal{H}c_e\delta' - 3\mathcal{H}'w_d\delta - 3\mathcal{H}w'_d\delta \\ &- 3\mathcal{H}w_d\delta' = 3w'_d\phi' + 3(1+w_d)\phi'' . \end{aligned} \quad (\text{A3})$$

Now from Eq. (7)

$$\theta' = -\mathcal{H}(1-3w_d)\theta - \frac{w'_d}{1+w_d}\theta + k^2\frac{c_e\delta}{1+w_d} + 3\mathcal{H}(c_e - c_a)\theta + k^2\phi, \quad (\text{A4})$$

and from Eq. (6)

$$\theta = 3\phi' - \frac{\delta'}{1+w_d} - \frac{3\mathcal{H}c_e\delta}{1+w_d} + \frac{3\mathcal{H}w_d\delta}{1+w_d}. \quad (\text{A5})$$

Substituting Eqs. (A4) and (A5) into Eq. (A3), we have a second order equation governing the evolution of DE. Changing the independent variable to the scale factor, the coefficients in Eqs. (12) can be retrieved. On the other hand if we consider  $\frac{\delta p}{\delta \rho} = c_e$  and ignore

the second term in Eq. (A2), we find

$$\begin{aligned}
 A_d &= \frac{1}{a} \left[ 2 + \frac{\mathcal{H}'}{\mathcal{H}^2} + 3c_e - 6w_d \right] , \\
 B_d &= \frac{1}{a^2} \left[ 3(c_e - w_d) \left( 1 + \frac{\mathcal{H}'}{\mathcal{H}^2} - 3w_d \right) + \frac{k^2}{\mathcal{H}^2} c_e - 3a \frac{dw_d}{da} \right] , \\
 S_d &= (1 + w_d) \left[ 3 \frac{d^2\phi}{da^2} + \frac{3}{a} \left( 2 + \frac{\mathcal{H}'}{\mathcal{H}^2} - 3w_d \right) \frac{d\phi}{da} \right. \\
 &\quad \left. - \frac{k^2}{a^2 \mathcal{H}^2} \phi + \frac{3}{1 + w_d} \frac{d\phi}{da} \frac{dw_d}{da} \right] ,
 \end{aligned}$$

which coincide with the values in Abramo et al. (2009) for  $w_d = \text{const}$  and  $\frac{\mathcal{H}'}{\mathcal{H}^2} = -\frac{1}{2}$  (matter dominated). We notice that for  $w_d = c_e = c_a = 0$  the coefficients for matter density contrast are recovered.

## APPENDIX B: POISSON EQUATION

On sub-horizon scales, the basic equation describing the evolution of linear matter fluctuations is

$$\ddot{\delta}_m + 2H(t)\dot{\delta}_m + \frac{k^2}{a^2}\phi = 0 . \quad (\text{B1})$$

In this context the Poisson equation in the Fourier space is written as (Lima et al. 1997)

$$k^2\phi = -4\pi G a^2(\delta\rho + 3\delta p) . \quad (\text{B2})$$

where  $\delta\rho = \delta\rho_m + \delta\rho_d$  and  $\delta p = \delta p_m + \delta p_d$ . Now using  $\delta p_m = 0$ ,  $\delta p_d = c_e\delta\rho_d$ ,  $\delta\rho_m = \rho_m\delta_m$ ,  $\delta\rho_d = \rho_d\delta_d$ , and inserting the above quantities into Eq.(B2), we arrive to

$$-\frac{k^2}{a^2}\phi = 4\pi G[\rho_m\delta_m + (1 + 3c_e)\rho_d\delta_d] , \quad (\text{B3})$$

or

$$-\frac{k^2}{a^2}\phi = \frac{3}{2}H^2[\Omega_m\delta_m + (1 + 3c_e)\Omega_d\delta_d] . \quad (\text{B4})$$

Utilising the above equations it is easy to check that

$$\ddot{\delta}_m + 2H(t)\dot{\delta}_m = \frac{3H^2}{2}[\Omega_m\delta_m + \Omega_d\delta_d(1 + 3c_e)] . \quad (\text{B5})$$

Obviously for  $c_e = w_d = \text{const}$ . the latter equation reduces to that of Abramo et al. (2009) and Mehrabi et al. (2015). Changing the variables from  $t$  to  $a$  we finally obtain Eq. (39).

This paper has been typeset from a  $\text{\TeX}/\text{\LaTeX}$  file prepared by the author.